Bifurcations and chaos in a coupled superconducting-quantum-interference-device ring–resonator system

T. D. Clark,* J. F. Ralph, R. J. Prance, H. Prance, J. Diggins, and R. Whiteman
Physical Electronics Group, School of Engineering, University of Sussex, Brighton, Sussex BN1 9QT, United Kingdom
(Received 3 November 1997)

In this paper we consider from a theoretical viewpoint the dynamical behavior of a superconducting-quantum-interference-device ring (a single Josephson weak link enclosed by a thick superconducting ring) in its ground state when coupled inductively to a radio frequency (rf) tank circuit resonator. We show that this simple system, when strongly driven at rf, displays a rich nonlinear dynamical structure, including unusual fold bifurcations and chaos. [S1063-651X(98)02904-3]

PACS number(s): 05.45.+b, 41.20.−q, 47.20.Ky, 85.25.Dq

I. INTRODUCTION

Over the years the nonlinear dynamics associated with circuits containing Josephson weak-link devices have been the focus of a great deal of attention. In particular, much work has been concentrated on the behavior of a simple superconducting-quantum-interference-device (SQUID) ring (a single Josephson weak link, capacitance C, enclosed by a thick superconducting ring, inductance Λ) inductively coupled to a parallel radio frequency (rf) LC resonant tank circuit [1–3]. This interest arises because of the nonlinear response of the screening supercurrent flowing in a SQUID ring to an external magnetic flux Φ_x, which, for finite coupling, is enhanced by the feedback between the ring and the tank circuit. In recent experimental work we have explored some of the rich nonlinear effects that can be generated in this apparently simple ring-tank circuit system when it is driven at rf. In this paper we consider in detail the theoretical model we have used to describe the system.

The screening current response of a SQUID ring can be conveniently categorized as reversible or irreversible in the external flux Φ_x, these two regimes of behavior being referred to, respectively, as inductive and hysteretic. In this work we will be concerned only with reversible responses, in the inductive (dissipation-less) mode, in which the screening current has an almost-sawtooth, Φ_0- $(=h/2e)$ periodic, dependence on Φ_x. These almost-sawtooth screening currents, which only recently have become accessible experimentally, generate very strong nonlinearities in ring-tank circuit systems. We can calculate (as a lookup table) the form of an almost-sawtooth screening current response by solving the time-independent Schrödinger equation (TISE) for the ground state $(\kappa=0)$ of a SQUID ring using the well-known lumped component ring Hamiltonian [4]

$$H=\frac{Q^2}{2C}+\frac{(\Phi-\Phi_x)^2}{2\Lambda}-\hbar\nu\cos\left(2\pi\frac{\Phi}{\Phi_0}\right), \qquad (1.1)$$

where the SQUID conjugate variables are Φ, the magnetic flux threading the ring, and Q, the total displacement flux across the weak link; here $\hbar\nu/2$ is the matrix element for Josephson pair tunneling through the weak link (critical current $I_c=2e\nu$). Solving the TISE yields the energy eigenvalues $E_\kappa(\Phi_x)$ of the SQUID ring (i.e., the low-energy macroscopic excitations of the ring modes) for levels $\kappa=0$ (ground state), $\kappa=1$ (first excited state), etc. The ring screening current is then given by the first derivative $\langle I_s(\Phi_x)\rangle_\kappa = -\partial E_\kappa(\Phi_x)/\partial\Phi_x$ with the second derivative yielding the magnetic susceptibility of the ring, i.e., $\chi_\kappa(\Phi_x) = -\Lambda\partial^2 E_\kappa(\Phi_x)/\partial\Phi_x^2$. In this description almost-sawtooth ground-state screening current patterns develop when the energy separation between the ground and first excited states $\Delta E_{01}[\Phi_x=(n+\frac{1}{2})\Phi_0]$ is small, where n is an integer. As an example, we show in Fig. 1 the ground-state current pattern found by solving the ring TISE for the typical experimental parameters $\hbar\nu=0.06\Phi_0^2/\Lambda$ and $\hbar/\sqrt{\Lambda C}=\hbar\omega_0 = 0.043\Phi_0^2/\Lambda$. Here $\Delta E_{01}[(n+\frac{1}{2})\Phi_0]=500$ GHz, i.e., extremely large on the scale of the drive frequency (around 20 MHz) considered in our calculations. In this paper, which is concerned with modeling such rf-driven SQUID rings at a few degrees kelvin, we therefore consider only the adiabatic ground state of the ring.

II. NONLINEAR DYNAMICAL DESCRIPTION

Our model system comprises a SQUID ring (weak-link capacitance C and ring inductance Λ) that is coupled to a

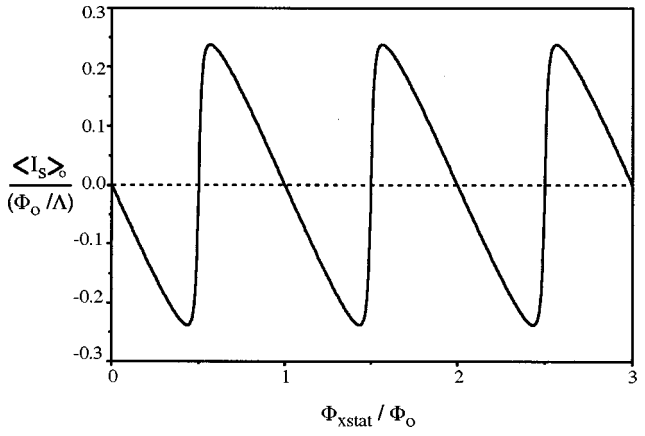

FIG. 1. Ground-state screening current response of a SQUID ring found by solving the TISE for the ring parameters $\hbar\nu = 0.06\Phi_0^2/\Lambda$, $\hbar/\sqrt{\Lambda C}=\hbar\omega_0=0.043\Phi_0^2/\Lambda$, and $\Lambda=3\times10^{-10}$ H.

*Electronic address: t.d.clark@sussex.ac.uk

measurement circuit resonator (the tank circuit), with a system quality factor Q. Starting from the quantum ground state of the ring, the nonlinear equation of motion for this coupled system is [5]

$$C_t \frac{d^2\varphi}{dt^2} + \frac{1}{R_t}\frac{d\varphi}{dt} + \frac{\varphi}{L_t} = I_{\rm in}^{\rm coh}\cos(\omega_{\rm rf}t+\delta) + I_{\rm in}^{nz}(t) + \mu\langle I_s(\mu\varphi+\Phi_x)\rangle_\kappa, \quad (2.1)$$

where, for simplicity, $\delta=0$. Here L_t and C_t are the tank circuit inductance and capacitance, respectively, $\omega_R/2\pi$ $(=1/2\pi\sqrt{L_tC_t})$ is the bare tank circuit resonance frequency, R_t is the tank circuit resistance on parallel resonance, φ is the rf flux in the tank circuit coil, $\mu=M/L_t$ (for ring-tank circuit mutual inductance M) is the fraction of this rf flux coupled into the SQUID ring, and $I_{\rm in}^{\rm coh}$ and $I_{\rm in}^{nz}(t)$ are, respectively, the coherent and noise current terms driving the tank circuit. We note that the inductive coupling between the ring and the tank circuit is often given in terms of the flux coupling factor $K=[M^2/L_t\Lambda]^{1/2}=[\mu^2L_t/\Lambda]^{1/2}$. In passing we note that when the characteristic time for the tank circuit $(\tau_t = 2\pi\sqrt{L_tC_t})$ is very long on the characteristic time (τ_s) of the SQUID ring, the resistively shunted junction plus capacitance model [1,6] of the ring-tank circuit dynamics is essentially equivalent to the above [Eqs. (1.1) and (2.1)] description in which the ring, treated quantum mechanically in its ground state, is coupled to a classical resonator. With $\tau_s \simeq 1/(20\ \text{MHz})$ this is always the case in any physically realistic SQUID ring. Our preference for the quantum description to calculate the screening current is influenced by our experimental work on point contact SQUID rings, driven at rf. We have shown elsewhere that it is possible experimentally to access extremely small weak link capacitances (10^{-15} to 10^{-16} F) in these point-contact systems [7–10]. This makes a quantum-mechanical treatment appropriate given typical operating temperatures of a few degrees kelvin.

For the parameter ranges that interest us here, there are no analytic solutions to the SQUID ring equation (2.1) and it must be solved numerically. This we have done extensively and reported our results (see Refs. [11,12], for example). However, the experimentally relevant parameter space is vast and we make no claim to have made an exhaustive investigation of all the inherent nonlinear phenomena associated with it.

Our principal concern in this paper is to find the frequency response of the coupled ring-tank circuit system. This can be calculated using a procedure that mimics the function of a real swept frequency source spectrum analyzer. In practice, the spectrum analyzer provides a constant amplitude drive current to the tank circuit, which is independent of frequency. This is usually termed the tracking generator signal at frequency ω. The response of the circuit is then mixed out at this frequency. Given the constant drive current, ω is swept over the frequency range of interest and the system response (for us, the rf voltage across the tank circuit) is recorded.

Our method for modeling the experimental situation is as follows. We first set $I_{\rm in}^{\rm coh}=0$ so that the system is purely noise driven. We then integrate the equation, sampling $d\varphi/dt$ and calculating the power spectrum by fast Fourier transform. This enables us to locate the noise peak in frequency space and thus estimate a window over which we wish to determine the frequency response. We note here that this procedure only gives us a guide to the spectral region of interest since the thermal power spectrum and the frequency response can differ considerably (particularly for tracking generator signals that are substantially larger than the noise signal). Nonetheless, in practice this window estimation method works well.

Having established the spectral window of interest, we divide the region between $\omega_{\rm min}$ and $\omega_{\rm max}$ into N frequency values at $\omega_{\rm min}$, $\omega_{\rm min}+\delta\omega$, $\omega_{\rm min}+2\delta\omega,...,\omega_{\rm max}$. Starting at the lowest frequency, we set arbitrary initial conditions (typically $d\varphi/dt=\varphi=t=0$) and $\omega=\omega_{\rm min}$ and integrate Eq. (2.1) to obtain the power spectrum $P(\omega_{\rm min})$ by single-point Fourier transform for a chosen value of $I_{\rm in}^{\rm coh}$, where

$$P(\omega)=\lim_{S\to\infty}\frac{2}{S}\left|\int_0^S \frac{d\varphi}{dt}\,e^{i\omega t}dt\right|^2. \quad (2.2)$$

In terms of drive current periods $(2\pi/\omega)$, we typically take values of $S=M$ $(2\pi/\omega)$, where M is an integer and typically $M=10^2-10^4$ as an approximation to the limit.

Without resetting the initial conditions, we then increment the frequency so that $\omega=\omega_{\rm min}+\delta\omega$ and calculate $P(\omega_{\rm min}+\delta\omega)$ and likewise $P(\omega_{\rm min}+2\delta\omega),...,P(\omega_{\rm max})$, thereby building up the frequency response from left to right. Having done so, we then decrement the frequency calculating $P(\omega_{\rm max})$, $P(\omega_{\rm max}-\delta\omega)$, $P(\omega_{\rm max}-2\delta\omega),...,P(\omega_{\rm min})$.

We find that the results obtained do not depend crucially on the initial conditions set at $\omega_{\rm min}$, but that the ''history'' in the calculation as we sweep one way and then back means that the left-to-right frequency response may not be identical to the right-to-left frequency response if multiple solutions to the equation exist. It is worth pointing out that the chosen value $I_{\rm in}^{\rm coh}$ of the tracking generator does dramatically influence the results. We like to refer to the tracking generator signal in terms of the $\mu\Phi_{\rm rms}$ that couples to the SQUID. There is no simple analytic relationship between $I_{\rm in}^{\rm coh}$ and $\mu\Phi_{\rm rms}$ [11], but $\mu\Phi_{\rm rms}$ can be calculated at the same time as the frequency response. For a given screening current response $\langle I_s(\Phi_x)\rangle_\kappa$ (which can be calculated for a given κ state, $\hbar\omega_0$, and $\hbar\nu$) our (left-to-right and right-to-left) frequency response curves are determined by the parameters ω_R, Q, $I_{\rm in}^{\rm coh}$, μ, and Φ_x. We note that since $\langle I_s(\Phi_x)\rangle_\kappa$, which is responsible for nonlinear behavior in the frequency response, is Φ_0 periodic in Φ_x, the frequency response also has the same flux periodicity.

We recently reported the observation of bistabilities in the SQUID-ring–tank circuit system that lead to apparently discontinuous changes in the frequency response [13]. Weak (cyclic fold) bifurcations of this general form were predicted by Likharev [14] using perturbative analytical methods. In this paper we solve the full nonlinear equation of motion (2.1), accurate to all orders. Because of the computational demands of this problem our first report concentrated on the external flux values $\Phi_x=(n+\frac{1}{2})\Phi_0$ and $n\Phi_0$ (for integer n), where we showed that a folding of the resonance curve occurs at moderately large tracking generator signals ($\mu\Phi_{\rm rms} \simeq \Phi_0$). This folding (as reported [13]) was seen to be to-

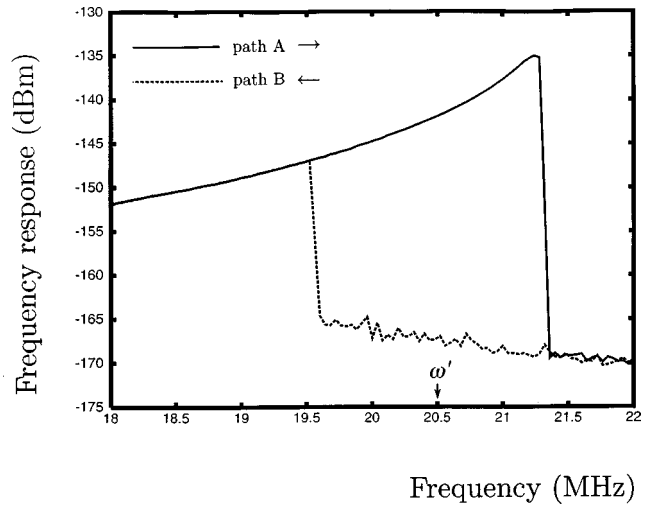

FIG. 2. Frequency response for $\Phi_x=(n+\frac{1}{2})\Phi_0$, where n is an integer, with the parameters $\hbar\omega_0=0.043\Phi_0^2/\Lambda$, $\hbar\nu=0.06\Phi_0^2/\Lambda$, $\omega_R/2\pi=21.0035$ MHz, $\mathbb{Q}=100$, $I_{\rm in}^{\rm coh}=22.61$ nA, $\mu=1.496\times10^{-2}$, and $T=4.2$ K; here $\omega'/2\pi=20.5$ MHz.

wards the right at $\Phi_x=(n+\frac{1}{2})\Phi_0$ and towards the left at $\Phi_x=n\Phi_0$. In Fig. 2 we show a similar example, where we have used typical experimental parameter values for the coupled system, namely, $\hbar\omega_0=0.043\Phi_0^2/\Lambda$, $\hbar\nu=0.06\Phi_0^2/\Lambda$, $\omega_R/2\pi=21.0035$ MHz, $\mathbb{Q}=100$, $I_{\rm in}^{\rm coh}=22.61$ nA, $\mu=1.496\times10^{-2}$, $T=4.2$ K, and $\Phi_x=(n+\frac{1}{2})\Phi_0$. Examples of such folding effects are well known in other areas of nonlinear dynamics [15,16], but here it has been observed in coupled SQUID-ring–tank circuit systems.

III. CHAOS IN THE FOLDING

The appearance of fold regions indicates that two stable solutions to the equation exist. To reveal these solutions we choose a frequency within the fold region such as that indicated by ω' in Fig. 2. For a given initial condition we then integrate Eq. (2.1) for several $\times\mathbb{Q}$ periods of ω' to allow transients to die out, after which we plot the phase plane $d\varphi/dt$ vs φ. By repeatedly doing this for randomly chosen initial conditions we may reveal in the phase plane the solutions that exist to the equation. An example is shown in Fig. 3(a), where we clearly see a large periodic solution corresponding to path A on the resonance curve of Fig. 2, and a smaller chaotic solution, enlarged in Fig. 3(b), corresponding to path B in Fig. 2 [the parameter $g=\sqrt{1-K^2\chi(\Phi_x)}|_{\Phi_x=0}$ in Fig. 3 is used for our own calculational convenience]. We can verify the chaotic nature of this smaller solution by calculating the Lyapunov exponents of the system. These exponents give a measure of the average amount of stretching and folding that occurs and is typical of chaotic systems. For a second-order differential equation such as Eq. (2.1), there are three Lyapunov exponents corresponding to the three degrees of freedom t, φ, and $d\varphi/dt$ in the phase space. One of these exponents is zero, reflecting the absence of expansion or contraction along the time axis with respect to arbitrarily close initial conditions. Either the remaining two are both negative (for the case of a periodic attractor) or one is negative and the other positive (for the case of a chaotic attractor). Chaos is defined by the presence of a positive Lyapunov

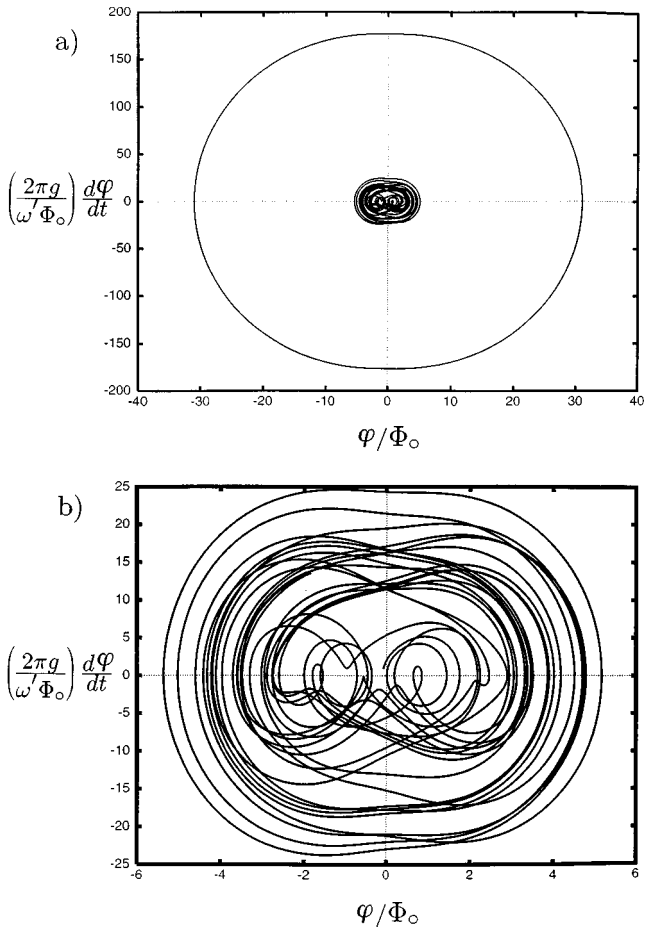

FIG. 3. Phase plane $d\varphi/dt$ vs φ (in normalized units) of Fig. 2 at frequency ω' along (a) path A and (b) path B.

exponent. For a dissipative system such as ours, there is a further constraint, which is that the sum of the exponents must be negative. Details about the origin, nature, and methods of the determination of Lyapunov exponents can be found in Refs. [17–20].

In Fig. 4 we show the Lyapunov exponents as a function of frequency corresponding to the frequency response curves of Fig. 2. In Fig. 4(a) we show the exponents for the left-to-right sweep (A) in Fig. 2 and in Fig. 4(b) we show the exponents for the right-to-left sweep (B) in the same figure. For clarity the trivial zero exponents are not shown.

In both Figs. 4(a) and 4(b) we see that on the low-frequency side of the fold the exponents are $(-,0,-)$, indicating a periodic solution. On the high-frequency side of the fold both Figs. 4(a) and 4(b) show exponents $(-,0,+)$, indicating chaotic solutions. In the fold region itself (the center region), Fig. 4(a) shows exponents $(-,0,-)$, which means that path A shown in Fig. 2 is due to a periodic solution (cf. the larger orbit in Fig. 3). Correspondingly, Fig. 4(b) exhibits exponents $(-,0,+)$ in this region, indicating that path B arises from chaotic solutions such as that shown in Fig. 2 (at frequency $\omega'=2\pi\times20.5$ MHz).

This pattern of behavior is all the more intriguing since the presence of chaos is not immediately apparent from the frequency response curve. The possibility of experimentally observing chaotic oscillations in the rf SQUID magnetometer was discussed from a theoretical viewpoint in some detail in

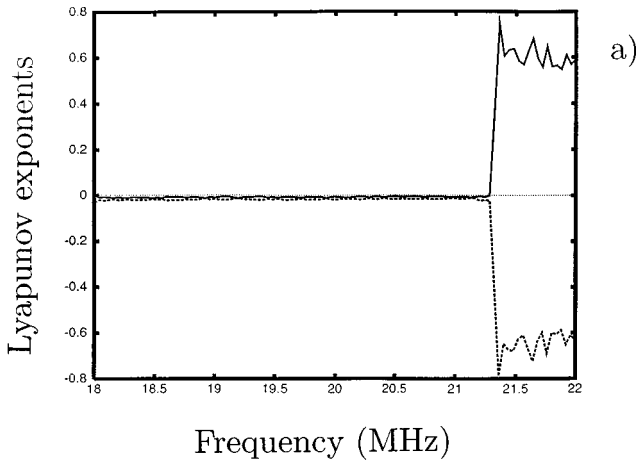

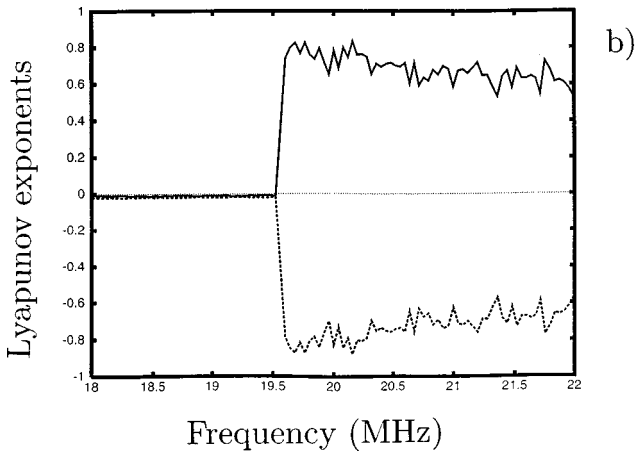

FIG. 4. Lyapunov exponents of Fig. 2 along (a) path *A* and (b) path *B*.

our Ref. [12]. The results presented here suggest that chaos is in fact accessible in experiments [13], but that it can easily be overlooked. It is worth pointing out that the circuit parameters that we have used here are quite typical of experimental ones.

IV. ATTRACTOR BASINS

The existence of two solutions means that a separatrix or basin-of-attraction boundary exists between the two. To reveal the structure of the separatrix, we use a Monte Carlo approach. Thus we select initial conditions at random and solve the equation to determine to which attractor the solution tends. In our case the separatrix is, in fact, three dimensional, but we choose to fix the initial time $t=0$ and look at a cross section of the basin of attraction. In Fig. 5 we show the results of such a calculation (at ω' and for the circuit parameters of Fig. 2). The dots indicate initial conditions that gravitate to the chaotic solution. The blank region contains points that gravitate to the periodic solution, but, for clarity, these have been omitted from the figure.

The separatrix itself is formed by the boundary between these sets of points and its spiral structure indicates the existence of a saddle point. Integrating Eq. (2.1) forward in time, the separatrix acts as a repellor such that initial conditions arbitrarily close to it are repelled away to one of the two stable solutions. By reversing the direction of time in the integration, repellors become attractors and vice versa. Integrating backward in time, all paths are repelled from the chaotic and periodic attractors and gravitate towards the separatrix. The spiral nature of the separatrix means that when the direction of time is reversed all paths fly off to infinity. Hence there are no stable solutions in the reversed time direction. This implies that a saddle point exists on the separatrix that is unstable in both the forward and reverse time directions.

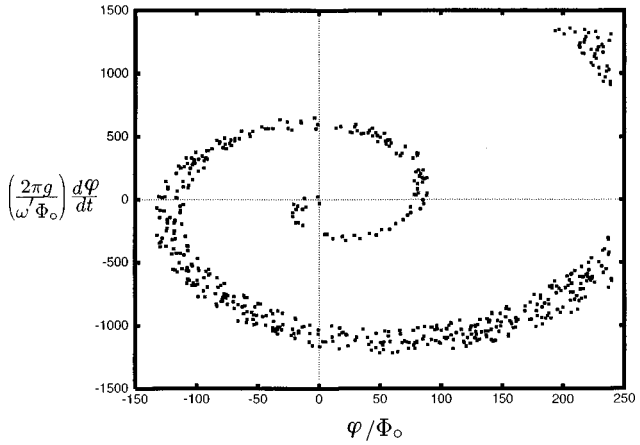

FIG. 5. Basins of attraction of Fig. 2 in the $d\varphi/dt$ vs φ plane at frequency $\omega'/2\pi = 20.5$ MHz.

Figure 6 shows another example of this effect for the same circuit parameters, but at $\Phi_x = n\Phi_0$. The frequency response shown in Fig. 6 exhibits a similar fold, but with the opposite orientation. There are no positive Lyapunov exponents corresponding to this frequency response, so that all paths are attributable to periodic solutions to the equation. All the circuit parameters that we have performed calculations for at $\Phi_x = n\Phi_0$ have this property, i.e., chaotic solutions do not appear to arise at this value of static external flux. This is entirely consistent with our previous findings on the chaotic dynamics of this system (other than where the

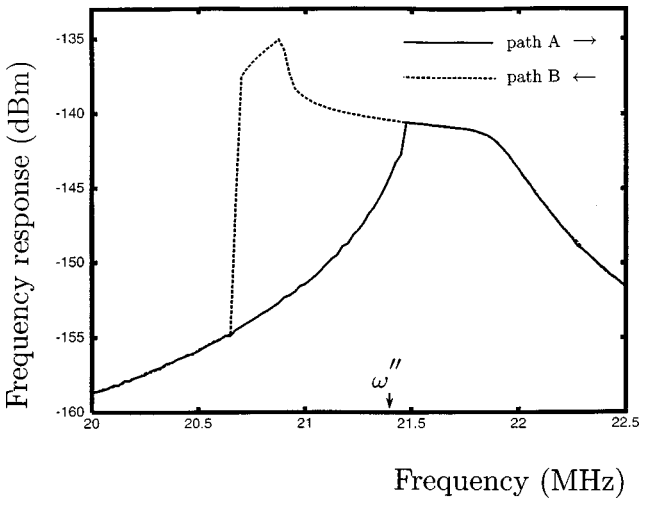

FIG. 6. Frequency response for the same parameters as in Fig. 2, but with $\Phi_x = n\Phi_0$, where n is an integer.

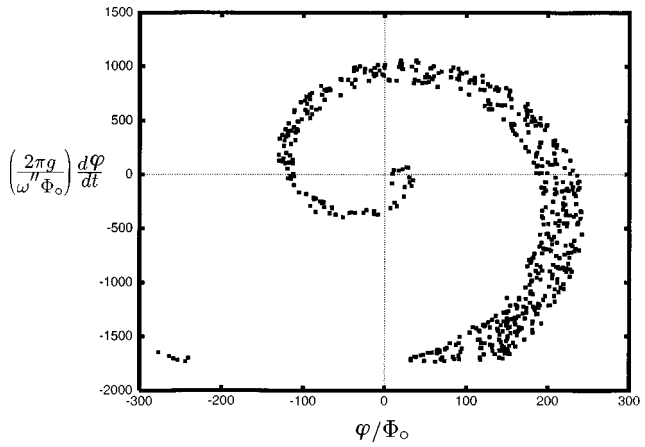

FIG. 7. Basins of attraction of Fig. 6 in the $d\varphi/dt$ vs φ plane at frequency $\omega''/2\pi = 21.4$ MHz.

screening current function is a discontinuous sawtooth and at exceptionally high coupling strengths) [12]. There are, however, two of these periodic solutions within the fold. For example, at frequency $\omega'' = 2\pi \times 21.4$ MHz, in Fig. 6 there are two solutions with orbits that differ in magnitude in a similar fashion to those of Fig. 3(a). Figure 7 shows the basins of attraction at the frequency ω'' in Fig. 6. The dots represent initial conditions that gravitate to the solution on path *A* in Fig. 6. The blank regions contain points that gravitate to the solution on path *B* although, as before, these have been omitted from the figure for the sake of clarity. Once again the spiral structure indicates the presence of a saddle point. A curious property of the system is revealed here since the separatrix spirals of Figs. 5 and 7 have the opposite orientation. This also indicates that it is not merely the presence of chaos that gives rise to the spiral in Fig. 5.

V. OPPOSED (HAMMERHEAD) BIFURCATIONS

We now extend our investigation to solve Eq. (2.1) for intermediate values of the external flux, i.e., $n\Phi_0 < \Phi_x < (n + \frac{1}{2})\Phi_0$. In Fig. 8 we show the frequency response curves

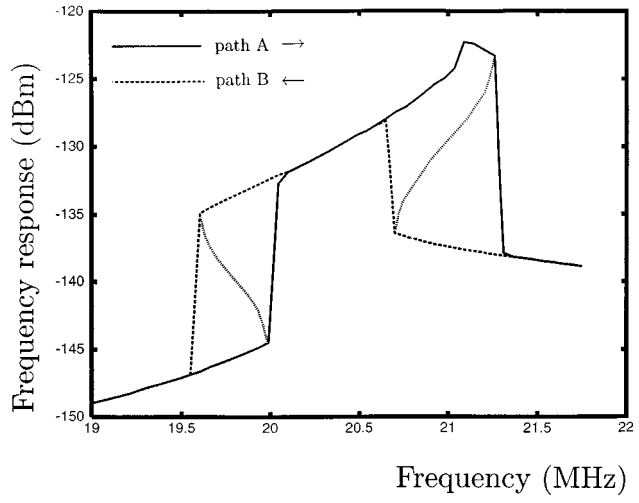

FIG. 8. ''Hammerhead'' frequency response for the same parameters as in Fig. 2, but with $\Phi_x = 0.625\Phi_0$.

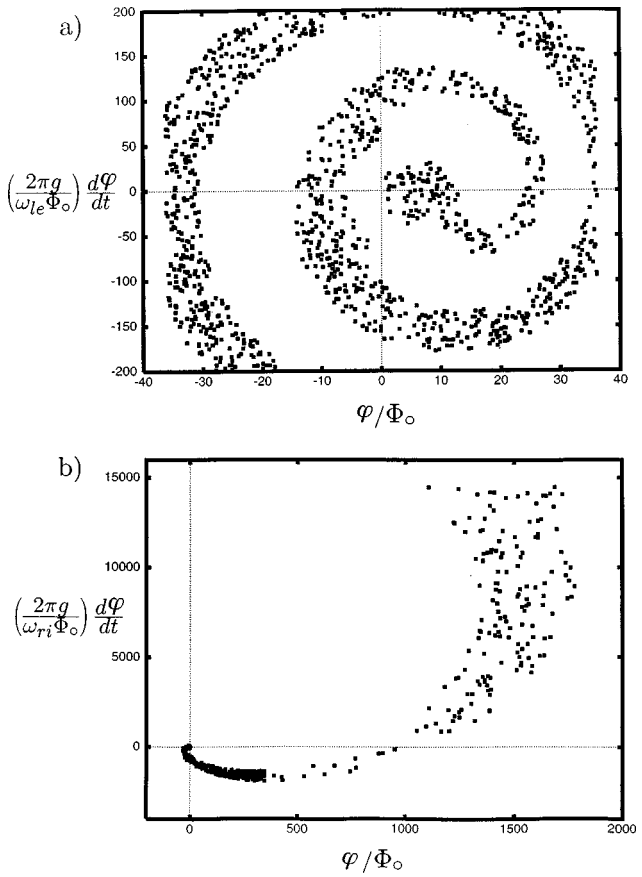

FIG. 9. Basins of attraction of Fig. 8 in the $d\varphi/dt$ vs φ plane at frequencies (a) $\omega_{le}/2\pi = 19.75$ MHz and (b) $\omega_{ri}/2\pi = 20.9$ MHz.

for sweeping in both directions at $\Phi_x = 0.625\Phi_0$ for the same circuit parameters as the previous figures. This figure shows a truly remarkable nonlinear effect, where there are two opposed and strongly folded bifurcation regions. Weakly folded opposed bifurcations of this type were predicted earlier by Likharev [14]. The strongly folded bifurcations of Fig. 8 have been observed by us experimentally in a SQUID-ring–tank circuit system [21] driven at large ($\simeq \Phi_0$) rf amplitudes. Previously, nonlinear features had been seen in the experimental resonance curves of SQUID-ring–tank circuit systems, but no folds, either singly or opposed [22,23]. The dotted lines drawn in Fig. 8 have been inserted to indicate the regions where saddle points exist. These lines do not represent solutions to the equation, but they are convenient for visualizing the fold structure. The similarity of the overall shape of the curve to an anvil or hammerhead is the reason why we have chosen the phrase ''hammerhead resonance'' to describe this effect. Similar behavior has been seen by Nayfeh, Nayfeh, and Pakdemirli [24], as a theoretical consideration. However, to our knowledge, this has never before been observed in an experiment.

The Lyapunov exponents corresponding to Fig. 8 are all less than or equal to zero, indicating that the underlying solutions are periodic. In Fig. 9 we show the basins of attraction corresponding to the frequencies (a) $\omega_{le} = 2\pi \times 19.75$ MHz and (b) $\omega_{ri} = 2\pi \times 20.9$ MHz. Again these reveal the spiraling structure associated with saddle points. We see here that the spirals have the same handedness as that in Fig. 5, although the tightness of the spiraling is markedly

different for Figs. 9(a) and 9(b). The concentration of points around the origin of the spiral in Fig. 9(b) is due to the fact that this figure contains points from two Monte Carlo runs over different search ranges. The figure suggests that the spiral unfolds towards the high-frequency side of the response.

ACKNOWLEDGMENTS

We would like to thank the Engineering and Physical Sciences Research Council for its generous funding of this work. We would also like to thank Professor P. McClintock, Professor G. King, and Dr. J. Ilichev for helpful discussions.

[1] W. C. Schieve, A. R. Bulsara, and E. W. Jacobs, Phys. Rev. A **37**, 3541 (1988).
[2] A. R. Bulsara, J. Appl. Phys. **60**, 2462 (1986).
[3] M. P. Soerensen, M. Barchelli, P. L. Christiansen, and A. R. Bishop, Phys. Lett. **109A**, 347 (1985).
[4] T. P. Spiller, T. D. Clark, R. J. Prance, and A. Widom, in *Progress in Low Temperature Physics* edited by D. F. Brewer (North-Holland, Amsterdam, 1992), Vol. XIII.
[5] J. F. Ralph, T. P. Spiller, T. D. Clark, R. J. Prance, and H. Prance, Int. J. Mod. Phys. B **8**, 2637 (1994).
[6] See, for example, A. Barone, and G. Paterno, *Physics and Applications of the Josephson Effect* (Wiley, New York, 1982), Chap. 13; see also J. C. Gallop, *SQUIDS, The Josephson Effects and Superconducting Electronics* (Hilger, Bristol, 1991).
[7] H. Prance, R. J. Prance, T. P. Spiller, T. D. Clark, A. Clippingdale, J. Ralph, J. Diggins, and A. Widom, Phys. Lett. A **181**, 259 (1993).
[8] J. F. Ralph, T. D. Clark, R. J. Prance, H. Prance, and J. Diggins, J. Phys.: Condens. Matter **8**, 10 753 (1996).
[9] J. F. Ralph, T. D. Clark, J. Diggins, R. J. Prance, H. Prance, and A. Widom, J. Phys.: Condens. Matter **9**, 8275 (1997).
[10] T. P. Spiller, T. D. Clark, R. J. Prance, H. Prance, A. Widom, and Y. Srivastava, Nuovo Cimento B **107**, 725 (1992).
[11] J. F. Ralph, T. P. Spiller, T. D. Clark, R. J. Prance, and H. Prance, Phys. Lett. A **180**, 56 (1993).
[12] J. Diggins, J. F. Ralph, T. P. Spiller, T. D. Clark, H. Prance, and R. J. Prance, Phys. Rev. E **49**, 1854 (1994).
[13] R. Whiteman, J. Diggins, V. Schöllmann, G. Buckling, T. D. Clark, R. J. Prance, H. Prance, J. F. Ralph, and A. Widom, Phys. Lett. A **226**, 275 (1997).
[14] See the discussion in K. K. Likharev, *Dynamics of Josephson Junctions and Circuits* (Gordon and Breach, Sydney, 1986), pp. 490–494
[15] J. M. T. Thompson and H. B. Stewart, *Non-linear Dynamics and Chaos* (Wiley, New York, 1991), p. 125.
[16] P. G. Drazin, *Nonlinear Systems* (Cambridge University Press, Cambridge, 1992), p. 222.
[17] J. D. Farmer, Physica D **4**, 366 (1982).
[18] J. D. Farmer, Physica D **7**, 153 (1983).
[19] A. Wolf, J. B. Swift, H. L. Swinney, and J. A. Vastano, Physica D **16**, 285 (1985).
[20] See, for example, R. C. Hilborn, *Chaos and Non-linear Dynamics* (Oxford University Press, New York, 1994).
[21] R. Whiteman, J. Diggins, V. Schöllmann, T. D. Clark, R. J. Prance, H. Prance, and J. F. Ralph, Phys. Lett. A **234**, 205 (1997).
[22] V. I. Shnyrkov, V. A. Khlus, and G. M. Tsoi, J. Low Temp. Phys. **39**, 477 (1980).
[23] J. G. Park, Physica B & C **107B**, 745 (1981).
[24] A. H. Nayfeh, S. A. Nayfeh, and M. Pakdemirli, in *Non-linear Dynamics and Stochastic Mechanics*, edited by W. Klienmann and N. Sri Namachchivaya (CRC, Boca Raton, FL, 1995), p. 190.